sciendo

LATVIAN JOURNAL OF PHYSICS
AND TECHNICAL SCIENCES
2022, N 5

DOI: 10.2478/lpts-2022-0036

FIBRE OPTICAL COUPLER SIMULATION BY COMSOL MULTIPHYSICS SOFTWARE

E. Elsts[1*], A. Supe[2], S. Spolitis[2], K. Zakis[2], S. Olonkins[3],
A. Udalcovs[2], R. Murnieks[2], U. Senkans[2], D. Prigunovs[2,3],
L. Gegere[2,3], K. Draguns[4], I. Lukosevics[1], O. Ozolins[2],
J. Grube[1], V. Bobrovs[2]

[1]Institute of Solid State Physics, University of Latvia,
8 Kengaraga Str., Riga, LV-1063, LATVIA
[2]Institute of Telecommunications, Riga Technical University,
12 Azenes Str., Riga, LV-1048, LATVIA
[3]AFFOC Solutions,
2-58 Jaunibas Str., Kalnciems, LV-3016, LATVIA
[4]Institute of Atomic Physics and Spectroscopy, University of Latvia,
3 Jelgavas Str. - House of Science, Riga, LV-1004, LATVIA
*e-mail: edgars.elsts@cfi.lu.lv

The paper presents a simulation model developed for a special optical coupler intended for coupling radiation from signal and pump sources used for the realization of cladding-pumped doped fibre amplifiers. The model is developed in COMSOL Multiphysics and used to assess the pumping efficiency for different side pumping angles and different numbers of electromagnetic modes. The obtained results show that the highest pumping efficiency, above 75 %, is achieved for 5–14 modes when two fibres representing the pump source and the signal source form a 10-degree angle between their central axes. The search for the optimal number of modes corresponds to the development trend in optical coupler technology where the multimode pumping by light-emitting diode (LED) replaces the classical scheme with a single-mode pumping by a laser diode (LD).

Keywords: *COMSOL MULTIPHYSICS, double-clad fibre, optical coupler, side pumping.*

1. INTRODUCTION

Recently, cladding-pumped doped fibre amplifiers have attracted interest for application in space-division multiplexed (SDM) systems proving a transmission capacity increase in a cost-effective way [1], [2]. Hence, an appropriate amplifier is required for signal transmission over long distances (>100 km).

The most widely used optical amplifiers in telecommunications are the Erbium-Doped Fibre Amplifiers (EDFAs) and RAMAN effect based amplifiers. Optical signal amplification beyond optical C and L bands using doped fibre amplifiers is possible with other trivalent rare earth elements (ytterbium, thulium, neodymium, holmium, etc.) and their combinations. Co-doped fibre-based amplifiers are very promising solutions due to their low nonlinearity without degrading amplification efficiency [3]. For example, erbium combination with ytterbium allows increasing the distance between the erbium ions in the amplifying medium; therefore, co-doping with erbium/ytterbium minimizes the possibility of clustering of erbium, allowing for a higher concentration of erbium in the amplifying medium compared to the conventional implementation of erbium-doped fibres. As a result, shorter erbium/ytterbium-doped fibres are required to achieve a similar level of gain [4]. While for the Raman amplifiers pumping can be performed at any wavelength (i.e., there is no absorption band), and the signal characteristics are determined by optical phonon spectra in contrast to the rare-earth-doped fibre amplifiers, where the pump characteristics and signal bands are fixed [5].

The cladding pumping technique differs from the classic approach where pump light is coupled directly in the doped fibre core. Instead, high-power pump radiation is launched into a much larger inner cladding of double-cladding fibre. The pump light propagation regime in the inner cladding is highly multi-modal and therefore has a high probability of repeatedly crossing the core of double-cladding fibre. Once the pump reaches the core it is absorbed gradually by dopant ions, while the signal amplification process is the same as in the case of core pumping [6].

The key to optimal cladding-pumping performance is special double-clad fibre couplers [7]. These couplers ensure that signal is coupled into the output fibre core, but the pump light is guided into the inner cladding. Regarding cladding-pumping couplers, there are several possible realizations, for example, free space coupling (end pumping), tapered fibre bundles, geometrically multiplexed end-pumping, V-groove side pumping, shallow-angle side pumping, etc. For further studies, a shallow-angle side pumping scheme was chosen because of good characteristics in terms of efficiency, preservation of modal properties, and robust construction [8].

In addition to long-distance telecommunication networks, fibre optic couplers are used in various other areas, such as optical sensors in biophotonics [9], [10], combined optical coherence tomography and hyperspectral imaging in medicine [11], free-space optical communications [12], etc. Optimum performance of optical fibre amplifiers is also determined by the optical composition of optical fibres and their resistance to harsh environmental conditions [13]–[17].

An optical fibre amplifier consists of a doped fibre, one or more pump lasers, a passive wavelength coupler, which is also the

focus of this paper, optical isolators (Bragg grating (FBG) or Faraday rotator), and tap couplers (Fig. 1). The pump light is inserted into the rare-earth-doped fibre through a wavelength selective coupler where these schemes can be forward pumping (co-pumped), backwards-pumping (counter-pumped), or bidirectional-pumping (dual-pumped) [18], [19].

In forward pumping, the input signal and the pump signal propagate in the same direction inside the fibre; in back-pumping, the input signal and the pump signal propagate in opposite directions. Bidirectional pumping is performed in both directions simultaneously (Fig.1).

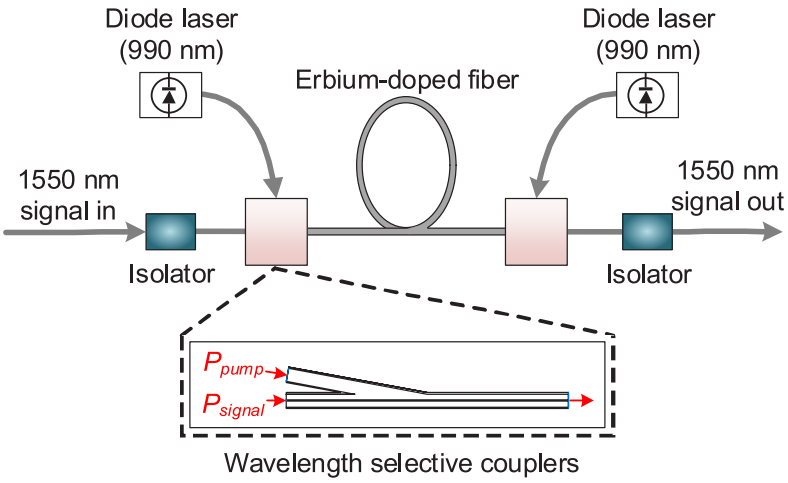

Fig. 1. Configuration of rare-earth-doped fibre amplifier employing a bidirectional pumping scheme.

Coupling efficiency is one of the most significant parameters that characterises a coupler. Because not all of the light from the pumping fibre is transferred to the information-carrying double-clad fiber. Coupling efficiency in fibre optics is the efficiency of optical power transfer between two optical components such as two optical fibres. Coupling efficiency is usually expressed as the ratio of output power to input power, converted to per cent [20], [21].

Coupling efficiency is determined by factors such as the optimal number of electromagnetic modes, the optimal angle between pumping and information-carrying fibres, etc. To the best of our attempt, no information was found about other studies performed by the COMSOL Multiphysics Software simulating the influence on coupler performance of these parameters.

The angle-polished method is efficient to connect pumping and information-carrying fibres. The efficiency of the coupler has been modelled by geometric optical methods analysing the light transmission in the core and inner cladding and the loss in the boundary between the inner and outer cladding of the double-clad fiber [22]. Multimode interference improves pumping efficiency through the reimaging effect to prevent light from diverging when exiting the fibre [23], [24].

Therefore, in this study, the number of electromagnetic modes is varied to find out at which number of modes the coupler reaches the highest efficiency.

For multimode pump fibre, to calculate coupling efficiency η_{lat} formulas [25], [26] could be applied. Lateral coupling efficiency is given by the formula:

$$\eta_{lat} \simeq \frac{16(n_1/n)^2}{[1+(n_1/n)^4}\frac{1}{\pi}\left\{2\cos^{-1}\left(\frac{y}{2a}\right)-\left(\frac{y}{a}\right)\left[1-\left(\frac{y}{2a}\right)^2\right]^{\frac{1}{2}}\right\}, \quad (1)$$

where n_1 is the refractive index of the core, n is the medium refractive index among the fibres, y is the lateral displacement of the axes of the fibre core and a is the radius of the fibre core.

Angular coupling efficiency is given by the formula:

$$\eta_{ang} \simeq \frac{16(n_1/n)^2}{[1+(n_1/n)]^4}\left[1-\frac{n\theta}{\pi n_1(2\Delta)^{\frac{1}{2}}}\right], \quad (2)$$

where Θ is the angular displacement in radians and Δ is the relative difference between the refractive indices of the fibre. The insertion loss due to angular misalignment may be obtained from the angular coupling efficiency in the same manner as the lateral misalignment loss following.

To combine multi-mode and single-mode fibre, a more complex simulation technique must be used for simulations. The most commonly used techniques are summarised below:

- In the effective-index method, a two-dimensional coupler structure is converted into an equivalent one-dimensional slab problem [27].
- The step-approximation method (Burns' method), where the amplitude transmission and mode conversion coefficients for the even and odd normal modes across the steps are rigorously obtained taking into account the phase difference between the two normal modes [28], [29].
- The finite-difference beam-propagation method (BPM) is a widely used algorithm for the solution of Maxwell's equations. It is applied to the eigenmode, propagating beam, and time-domain analyses of optical waveguides [30], [31].
- Finite Element Method (FEM) is a numerical technique that gives approximate solutions to differential equations that model problems arising in physics and engineering. As with the more commonly used finite difference schemes, the finite element method reduces problems defined in geometrical space (or domain) to find a solution in a finite number of points by subdividing the domain into smaller regions (a mesh) [32].

Further, the results of other authors who performed simulations similar to ours using the COMSOL Multiphysics software package are briefly described.

A coupling mechanism of a photoconductive terahertz antenna with radial symmetry was presented in [33]. The 3-D simulation domain is discretized into approximately 1.8 million tetrahedral mesh elements yielding a computational model consisting of 2.1 million degrees of freedom. The cylinder (2 cm diameter, 4 cm length) is placed such that its central axis lies at the centre of the gap between the waveguide and coupler wires. Part of the cylinder extends outside of the rectangular box, for a waveguide 15 cm long. The coupling efficiency of the scattering mechanism was 56 %–50 %.

The coupling efficiency was analysed [34] between the antenna and waveguide The excitation of gap plasmon waveguide (GPW) by dipole nanoantenna was simulated and results were compared with corresponding predictions obtained using standard antenna theory. The minimum mesh size was set to 3 nm. The size of the computational domain was always

3 μm × 3 μm × 3.5 μm. It was found that the use of nanoantennas could increase the conversion of an incident beam into a waveguide mode dramatically.

Non-volatile phase change materials (PCM) – clad silicon photonic 1 × 2 and 2 × 2 switches –, which can be used for applications such as optical interconnects, neuromorphic computing, quantum computing, and microwave photonics, were demonstrated [35]. The grid size of the mesh in our simulation was set at 20 nm in dimensions. A study was performed on how to improve the efficiency of the coupler.

In [36], a technique for the highly stable and efficient generation of radially TM01 and azimuthally TE01 polarized beams using weakly-fused fibre couplers was investigated. Based on the above analysis and the simulations shown, a conventional telecom-grade SMF (Elliot Scientific, SMF-1300/1500 core/cladding diameter = 8.2/125 μm, NA = 0.14) was adiabatically pre-tapered at ∼1400 ºC to a radius of r ∼ 38.6±0.1 μm for exciting the TE01 mode (NTT-AT, Japan). The fundamental mode in the SMF is directly coupled to the TM01 or TE01 mode by appropriately phase matching the modes in the fibres resulting in an efficiency of ∼67 % and ∼85 %, and polarization purity of 70 % and 82 %, respectively.

Optical waves confined within high refractive index regions if flanked by adjacent low index regions for biological event monitoring were studied [37]. To obtain converged results, a 0.2 mm maximum mesh size in the piezoelectric material region, a 0.15 mm maximum mesh size in the cavity, and a 1 mm mesh size in the Perfectly Matched Layer (PML) region were used. Each imagined sample was 100 μm to quantify the extent and depth of optical confinement in the cylindrical cavity (19 mm radius, 30 mm height). The input beam can be optimized to match the NA and maximize the coupling efficiency.

In the scheme presented by [38], a tapered nanofibre (TNF) was evanescently coupled with a substrate, allowing the pump light guided in the TNF to generate a strong transverse optical force for the light-control-light effect. The mesh sizes of the tapered nanofiber (TNF) and medium were 5 nm and 50 nm. The calculation space for the simulation was set as 7 μm × 9 μm × 60 μm and a TNF with a length of 60 μm was located at the centre of the calculation region along the z-direction.

In the study covered by this paper, based on data summarised in the above-mentioned publications, the numerical simulations of side coupling injection with the aid of COMSOL Multiphysics were performed to analyse its efficiency.

The rest of the manuscript is structured as follows: Section II describes the simulation methodology and input parameters of the modelled coupler as well as the obtained results. Finally, Section III provides a summary of the simulated results and concludes the paper.

2. METHODS AND RESULTS

The design of the coupler was simulated by COMSOL Multiphysics software using a two-dimensional model [39].

The 2D model was chosen as suitable because it required fewer computer resources and provided sufficient quality compared to the 3D model.

Electromagnetic field simulations were

performed using the Wave Optics Module of the software. The workflow can be described by the following steps:

- define the geometry;
- select materials;
- select a suitable Wave Optics interface;
- define the boundary and initial conditions;
- define the finite element mesh;
- select a solver;
- visualize the results.

To obtain characteristic values for calculating the electric and magnetic fields of the coupler, COMSOL Multiphysics built-in function *line integration* was used. This function evaluates a *line integration* value over the cut line in models of an electric and magnetic field. *Line integration* is expressed as the variable *normE,* which represents the amplitude of the electric field, and variable *normH,* which represents the amplitude of the magnetic field, respectively.

To describe the propagation of light in an optical fibre, power flow was examined using the time-averaged Poynting vector, which is the cross product of the electric field and the magnetic field:

$$\boldsymbol{S} = \frac{1}{2} Re(\boldsymbol{E} \times \boldsymbol{H}). \quad (3)$$

The studied coupler (shown in Fig. 2) has an information-carrying fibre (A) and pumping fibre (B) connected at an angle *g*, and a tapered section (C). Information-carrying fibre consists of single-mode (SM) core, an inner cladding, and an outer cladding. The pump fibre, respectively, consists of a multimode (MM) core and an outer cladding. Simulation parameters are given in Table 1.

Tab. 1. Fibre Parameters Used in our Simulations

Input and output fibre			**Pump fibre**		
Purpose	Diameter (μm)	Refractive index	Purpose	Diameter (μm)	Refractive index
SM core	5.8	1.5431	MM core	105	1.5293
SM inner cladding	105	1.5293	MM outside cladding	125	1.5054
SM outside cladding	125	1.5054			

The refractive indices of the core and claddings of the above-mentioned fibres were determined from commercially available double-cladding fibre with flower-shaped inner cladding. Scanning electron microscope (SEM) results of double cladding fibre showed the presence of phosphorus in the fibre core, which increased the refractive index of silica, the inner cladding was silica without any traces of rare-earth or additional dopant elements, and the outer cladding was made of fluorine-doped silica to reduce the refractive index of the material.

In our model, the length of information-carrying optical fibre is 2.25 mm and a pump fibre length is 1.12 mm. The reason for choosing such dimensions is the trade-off between the ability to easily monitor the model by software and the calculation time. The functional scheme of the coupler model is shown in Fig. 2.

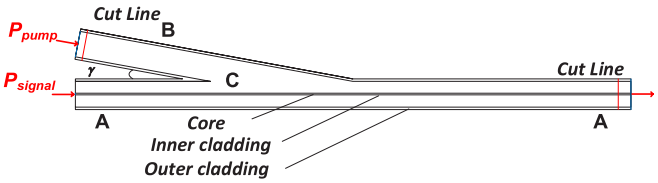

Fig. 2. Functional scheme of the coupler (information-carrying SM optical fibre (A) and pumping MM fibre (B) connected at an angle *g*, a tapered section (C), red-coloured cut lines indicate the location for line integration calculation).

The information-carrying optical signal is modelled taking into account an expected optical signal power: P_{sign}>1 mW at wavelength λ_{sign}=1550 nm and a pumping signal with power: P_{pump}=3W at wavelength λ_{pump}=980 nm.

The finite element method (FEM) is mesh-dependent, which means smaller elements can provide better representation. The finite element mesh is used to subdivide the model into smaller domains called elements, over which a set of equations is solved.

In our models, the mesh type was selected as "boundary layers", which was characterised by a dense distribution of elements in the normal direction along specific boundaries. Element size parameters – maximum element size: 2.25 μm, minimum element size: 0.225 μm, maximum element growth rate: 1.08, curvature factor: 0.25, and resolution of narrow regions: 1. This is a compromise between calculation quality and calculation time.

In our initial simulation, the signal with P_{sign}>1 mW at wavelength λ_{sign}=1550 nm was injected only in single-mode optical fibre (Fig. 3).

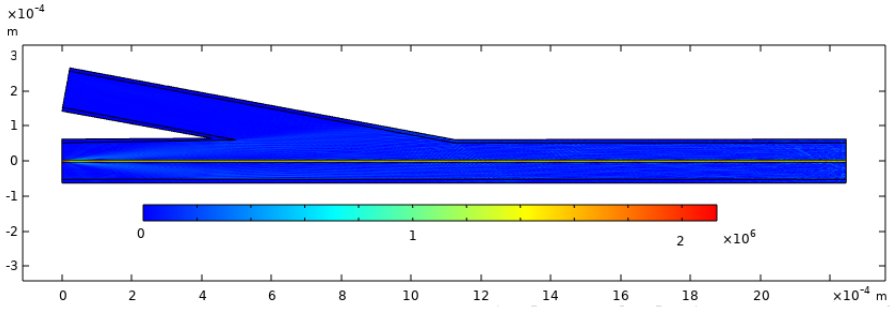

Fig. 3. The simulation of the signal propagating through the coupler (single-mode fibre core). Colours correspond to the strength of the electromagnetic field.

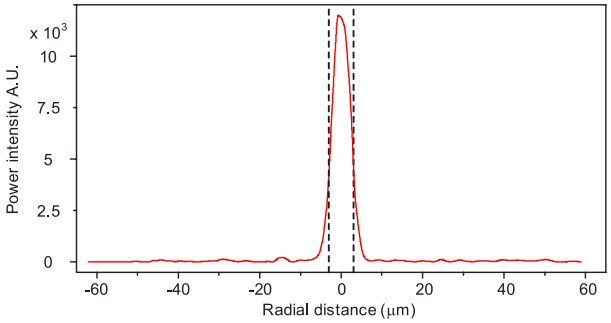

Fig. 4. A section of single-mode signal fibre shows an increase in intensity at the core of the fibre. Black dashed lines indicate fibre core diameter.

As shown in Fig. 3, the colour of the core is closer to red, indicating a more intense signal, and the other parts are blue, indicating the absence of signal. Figure 4 shows the electromagnetic field intensity dependence on the radial distance from the centre. The electromagnetic field intensity is represented by a red solid line, and the core diameter (5.8 μm) is represented by black dashed lines. The strongest signal is in the core of the fibre and a transitional region is observable on the border between core and cladding. *Cut line* locates at a distance of $16 \cdot 10^{-4}$ m from the beginning of the double cladding fibre (after connection pumping and signal fibres). Signal parameters in single-mode fibre do not change significantly as the signal propagates.

The part of the single-mode fibre that carries most of the light energy is larger than the core diameter of this fibre (Fig. 4). This phenomenon is called the mode field diameter (MFD). The MDF depends on the wavelength, the radius of the core, and the indices of refraction of the core and the cladding. The signal can be approximated by a Gaussian power distribution.

The next step in our simulations is the injection of the pumping signal with the power P_{pump}=3 W at wavelength λ_{pump}=980 nm into a multimode fibre.

The pump efficiency was analysed as a function of the connection angle between pumping fibre and the signal fibre at angles of 5°, 10°, 20° and 30°.

A 10-mode pumping signal was used. At an angle of 5°–10° coupler efficiency is about 95 %, but as the angle increases to 20°–30° degrees, the efficiency decreases rapidly to 2–5 %. The model with a 10° angle between the signal and the pumping fibre (Fig. 2) is found to be optimal because at a smaller angle the pumping signal tends to propagate backwards.

The optimal coupling angle of 5º–10º calculated by COMSOL Multiphysics agrees with the angle of 10º published in [40], where calculations were done using geometric optics with a step of 0.5 º and proved experimentally.

The dependence of the coupler efficiency on the number of modes injected into the double-cladding multimode pumping fibre was modelled in our study.

Coupling efficiency was assumed as the ratio of the power near the beginning of multimode pumping fibre, which was coupled into a single-mode double-clad fiber, and power registered near the end of double-clad fiber (see red-coloured *cut lines* in Fig. 2). *The line integration* function was used for numerical estimation.

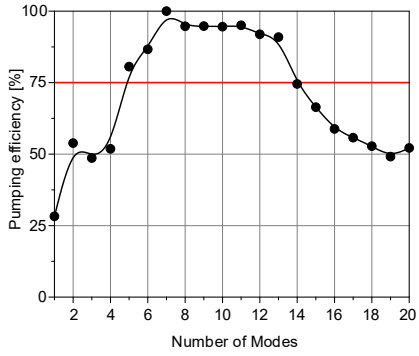

Fig. 5. Dependence of coupler efficiency on the number of electromagnetic modes.

The simulation shows the highest pumping efficiency with 7 electromagnetic modes, but it should be noted that the results would be more representative if the fibres were longer, but it would take more time to run such simulations.

The range of 5 to 14 electromagnetic modes was considered the most suitable, with an efficiency of over 75 %, as represented in Fig. 5. For instance, for the 50-mode model, only ~10 % pump efficiency can be achieved.

The power of the high-order modes leaks more than the power of low-order modes [41]–[43].

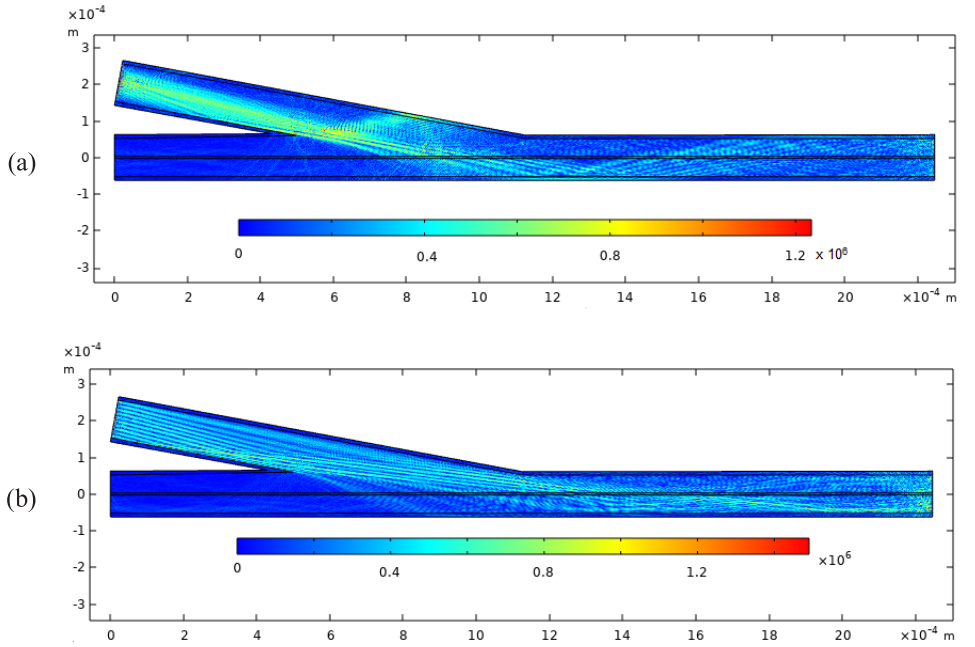

Fig. 6. The 2-dimensional coupler model in COMSOL Multiphysics forms a 10º angle between the pumping and the signal-carrying fibre with one (a) and ten (b) electromagnetic modes injected in the pumping fibre.

In Fig. 6, for illustration, one (a) and ten (b) modes are injected into a multimode pump fibre. The pump signal initially propagates almost parallel to the direction of the fibre, but entering the double-clad fibre starts to reflect from the outer coating. This pump signal propagation behaviour remains true in models with different number of modes which were calculated but not featured in this article.

In the research [44], the coupling efficiency as a function of the number of pumping modes was analysed using experimental data and Finite Difference Beam Propagation Method (FD-BPM) simulations. Pronounced peaks corresponding to 3 and 10 modes were observed, corresponding to multimode fibres with radii of 52.5 and 92.5 μm, respectively. That means the simulation model works correctly and our results are close to the already validated results. Note that recent overview of the current status of fibre-based multimode interference (MMI) devices with a particular focus on optical fibre-based sensing applications was presented in [45].

3. CONCLUSIONS

In this paper, an overview of couplers as an important component of amplifiers in optical communications networks was presented and useful results from the literature for coupler modelling with COMSOL Multiphysics software package were summarised.

A successful two-dimensional model simulating electric and magnetic fields in coupler with COMSOL Multiphysics software was developed, which showed that the optimum number of pumping modes lied in the range of 5 to 14 modes, which was similar to the previously reported results

but obtained by different methods.

The developed simulation methodology is an important step forward in the studies of optical couplers using the COMSOL Multiphysics environment. However, to test our simulation results experimentally the mode-filtering technique has to be applied. To accurately distinguish leakage from uncontrolled backward propagation additional experiments using FBG or Faraday rotation filters could be applied.

ACKNOWLEDGEMENTS

Funding: The research has been supported by the European Regional Development Fund project No.1.1.1.1/18/A/068.

The Institute of Solid State Physics, University of Latvia as a Center of Excellence has received funding from the European Union's Horizon 2020 Framework Programme H2020-WIDESPREAD-01-2016-2017-TeamingPhase2 under grant agreement No. 739508, project CAMART2.

REFERENCES

1. Puttnam, B. J., Rademacher, G., & Luís, R. S. (2021). Space-Division Multiplexing for Optical Fibre Communications. *Optica*, *8* (9), 1186–1203.
2. Yoshikane, N., & Tsuritani, T. (2020). Recent progress in space-division multiplexing optical network technology. In: *2020 International Conference on Optical Network Design and Modeling (ONDM)* (pp. 1–4). 18–21 May 2020, Barcelona, Spain, IEEE.
3. Aiso, K., Tashiro, Y., Suzuki, T., & Yagi, T. (2001). Development of Er/Yb Co-doped Fibre for High-Power Optical Amplifiers. *Furukawa Electric Review*, 35–39.
4. Supe, A., Olonkins, S., Udalcovs, A., Senkans, U., Mūrnieks, R., Gegere, L., … & Bobrovs, V. (2021). Cladding-Pumped Erbium/Ytterbium Co-Doped Fibre Amplifier for C-Band Operation in Optical Networks. *Applied Sciences*, *11* (4), 1702.
5. Selvarajan, A., Kar, S., & Srinivas, T. (2003). *Optical Fibre Communication: Principles and Systems*. Tata McGraw-Hill Education.
6. Filippov, V., Kerttula, J., Chamorovskii, Y., Golant, K., & Okhotnikov, O. G. (2010). Highly Efficient 750 W Tapered Double-Clad Ytterbium Fibre Laser. *Optics Express*, *18* (12), 12499–12512.
7. Lei, C., Chen, Z., Leng, J., Gu, Y., & Hou, J. (2017). The Influence of Fused Depth on the Side-Pumping Combiner for All-Fibre Lasers and Amplifiers. *Journal of Lightwave Technology*, *35* (10), 1922–1928.
8. Supe, A., Spolitis, S., Elsts, E., Murnieks, R., Doke, G., Senkans, U., ... & Bobrovs, V. (2020). Recent developments in cladding-pumped doped fibre amplifiers for telecommunications systems. In: *2020 22nd International Conference on Transparent Optical Networks (ICTON)* (pp. 1–6). 19–23 July 2020, Bari, Italy, IEEE.
9. Choi, I. S., Park, J., Jeong, H., Kim, J. W., Jeon, M. Y., & Seo, H. S. (2018). Fabrication of 4× 1 Signal Combiner for High-Power Lasers Using Hydrofluoric Acid. *Optics Express*, *26* (23), 30667–30677.
10. Zhu, X., Wang, K., Wang, F., Zhao, C., & Cai, Y. (2018). Coupling Efficiency of a Partially Coherent Radially Polarized Vortex Beam into a Single-Mode Fibre. *Applied Sciences*, *8* (8), 1313.
11. Guay-Lord, R., Attendu, X., Lurie, K. L., Majeau, L., Godbout, N., Bowden, A. K., ... & Boudoux, C. (2016). Combined Optical Coherence Tomography and Hyperspectral Imaging Using a Double-Clad Fibre Coupler. *Journal of Biomedical Optics*, *21* (11), 116008.

12. Dikmelik, Y., & Davidson, F. M. (2005). Fibre-Coupling Efficiency for Free-Space Optical Communication through Atmospheric Turbulence. *Applied Optics*, *44* (23), 4946–4952.
13. Eydi, N., Feghhi, S. A. H., & Jafari, H. (2021). Comprehensive Approach to Determination of Space Proton-Induced Displacement Defects in Silica Optical Fiber. *Nuclear Instruments and Methods in Physics Research Section B: Beam Interactions with Materials and Atoms*, *502*, 95–101.
14. Novoa, D., & Joly, N. Y. (2021). Specialty Photonic Crystal Fibers and Their Applications. *Crystals*, *11* (7), 739.
15. Ahmad, P., Khandaker, M. U., Rehman, F., Muhammad, N., Faruque, M. R. I., Ullah, Z., ... & Bradley, D. A. (2021). Facile Synthesis of High-Quality Nano-size 10B-Enriched Fibers of Hexagonal Boron Nitride. *Crystals*, *11* (3), 222.
16. Nathanael, A. J., & Oh, T. H. (2021). Encapsulation of Calcium Phosphates on Electrospun Nanofibers for Tissue Engineering Applications. *Crystals*, *11* (2), 199.
17. Fu, J., Chen, Y., Huang, Z., Yu, F., Wu, D., Pan, J., ... & Leng, Y. (2021). Photoionization-Induced Broadband Dispersive Wave Generated in an AR-filled Hollow-Core Photonic Crystal Fiber. *Crystals*, *11* (2), 180.
18. Itoh, T., Araki, T., Ashida, M., Iwata, T., Muro, K., & Yamada, N. (2011). Optical properties. In: *Springer Handbook of Metrology and Testing* (pp. 587–663). Springer, Berlin, Heidelberg.
19. Shukla, P., & Kaur, K. P. (2013). Performance Analysis of EDFA for Different Pumping Configurations at High Data Rate. *International Journal of Engineering and Advanced Technology (IJEAT)*, *2* (5), 487–490.
20. Standard, F. (1996). 1037C: *Telecommunications: Glossary of Telecommunication Terms*. National Communication System. Technology and Standards Division. Washington, DC: General Services Administration. Information Technology Service.
21. Chen, X., Xiao, Q. R., Jin, G. Y., Yan, P., & Gong, M. L. (2015). High Coupling Efficiency and Low Signal Light Loss (2+ 1)× 1 Coupler. *Chinese Physics B*, *24* (6), 064208.
22. Xiao, Q. R., Yan, P., Yin, S., Hao, J., & Gong, M. (2010). 100 W Ytterbium-Doped Monolithic Fibre Laser with Fused Angle-Polished Side-Pumping Configuration. *Laser Physics Letters*, *8* (2), 125.
23. Zhu, X., Schülzgen, A., Li, H., Li, L., Wang, Q., Suzuki, S., … & Peyghambarian, N. (2008). Single-Transverse-Mode Output from a Fibre Laser Based on Multimode Interference. *Optics Letters*, *33* (9), 908–910.
24. Pachon, E. G., Franco, M. A., & Cordeiro, C. M. (2012). Spectral bandwidth analysis of high sensitivity refractive index sensor based on multimode interference fiber device. In: *OFS2012 22nd International Conference on Optical Fiber Sensors* (vol. 8421, p. 84217Q). International Society for Optics and Photonics.
25. Miyazaki, K., Honda, M., Kudo, T., & Kawamura, T. (1975). Theoretical and experimental considerati ons of optical fibre connector. In: *Optical Fibre Transmission* (p. WA4). Optical Society of America.
26. Tsuchiya, H., Nakagome, H., Shimizu, N., & Ohara, S. (1977). Double Eccentric Connectors for Optical Fibres. *Applied Optics*, 16 (5), 1323–1331.
27. Knox, R. M., & Toulios, P. P. (1970). Integrated circuits for the millimeter through optical frequency range. In *Proc. Symp. Submillimeter Waves* (vol. 20, pp. 497–515). Brooklyn, NY.
28. Burns, W. K., & Milton, A. (1975) Mode Conversion in Planar-Dielectric Separating Waveguides. *IEEE Journal of Quantum Electronics, 11* (1), 32–39.
29. Okamoto, K. (1990). Theoretical Investigation of Light Coupling Phenomena in Wavelength-Flattened Couplers. *Journal of Lightwave Technology*, *8* (5), 678–683.

30. Shibayama, J., Yamauchi, J., & Nakano, H. (2003). Application of the finite-difference beam-propagation method to optical waveguide analysis. In: *17th International Conference on Applied Electromagnetics and Communications* (pp. 262–265). 1–3 October 2003, Dubrovnik, Croatia, IEEE.
31. Optiwave. (n.d.). *Optiwave Photonic Software*. Available at https:// www. optiwave. com/
32. Pepper, D. W., & Heinrich, J. C. (2017). *The Finite Element Method: Basic Concepts and Applications with MATLAB, MAPLE, and COMSOL*. CRC press.
33. Deibel, J. A., Wang, K., Escarra, M. D., & Mittleman, D. M. (2006). Enhanced Coupling of Terahertz Radiation to Cylindrical Wire Waveguides. *Optics Express,* 14 (1), 279–290.
34. Wen, J., Romanov, S., & Peschel, U. (2009). Excitation of Plasmonic Gap Waveguides by Nanoantennas. *Optics Express*, *17* (8), 5925–5932.
35. Xu, P., Zheng, J., Doylend, J. K., & Majumdar, A. (2019). Low-Loss and Broadband Nonvolatile Phase-Change Directional Coupler Switches. *Acs Photonics*, *6* (2), 553–557.
36. Pidishety, S., Srinivasan, B., & Brambilla, G. (2016). All-Fiber Fused Coupler for Stable Generation of Radially and Azimuthally Polarized Beams. *IEEE Photonics Technology Letters*, *29* (1), 31–34.
37. Chamanzar, M., Scopelliti, M. G., Bloch, J., Do, N., Huh, M., Seo, D., ... & Maharbiz, M. M. (2019). Ultrasonic Sculpting of Virtual Optical Waveguides in Tissue. *Nature Communications*, *10* (1), 1–10.
38. Zhang, Y., Zhu, W., Fan, P., He, Y., Zhuo, L., Che, Z., ... & Chen, Z. (2020). A Broadband and Low-Power Light-Control-Light Effect in a Fiber-Optic Nano-Optomechanical System. *Nanoscale*, *12* (17), 9800–9809.
39. Comsol. (n.d.). *Mach–Zehnder Modulator*. Available at thttps://www.comsol.com/model/mach-8211-zehnder-modulator-5061
40. Ou, P., Yan, P., Gong, M., & Wei, W. (2004). Coupling Efficiency of Angle-Polished Method for Side-Pumping Technology. *Optical Engineering*, *43* (4), 816–821.
41. Xiao, Q., Chen, X., Ren, H., Yan, P., & Gong, M. (2013). Fibre Coupler for Mode Selection and High-Efficiency Pump Coupling. *Optics Letters*, *38* (7), 1170–1172.
42. Fanlong, D., Xinhai, Z., & Feng, S. (2018). Side Coupler Applied in a Multi-Pumped Yb-Doped Triple-Clad Fibre Laser. *Laser Physics*, *28* (12), 125106.
43. Ou, P., Yan, P., Gong, M., Wei, W., & Yuan, Y. (2004). Studies of Pump Light Leakage out of Couplers for Multi-Coupler Side-Pumped Yb-doped Double-Clad Fibre Lasers. *Optics Communications*, *239* (4–6), 421–428.
44. Mohammed, W. S., Mehta, A., & Johnson, E. G. (2004). Wavelength Tunable Fibre Lens Based on Multimode Interference. *Journal of Lightwave Technology*, *22* (2), 469.
45. Guzmán-Sepúlveda, J. R., Guzmán-Cabrera, R., & Castillo-Guzmán, A. A. (2021). Optical Sensing Using Fiber-Optic Multimode Interference Devices: A Review of Nonconventional Sensing Schemes. *Sensors*, *21* (5), 1862.